Surface Effects on the Electrostatic Potential Generated in a Bent Gallium Nitride Nanowire

Jin Zhang, Chengyuan Wang, and Sondipon Adhikari

***Abstract*—The aim of this paper is to conduct the first study of the surface effects on the voltage output of bent gallium nitride (GaN) nanowires (NWs), which are promising for nanogenerators. To reach this goal, a 3-D composite beam model was developed and the corresponding theoretical framework was established for the structural responses of piezoelectric NWs. In this study molecular dynamics simulations (MDS) were first carried out to determine the exact material properties for several small NW samples. The MDS-derived size-dependence of parameters provide fitting points for the 3-D composite beam with a core-shell geometry. With the aid of the finite element techniques the equivalent material properties obtained from above fitting procedure enable the use of the core-shell model for larger structures where MDS were not feasible. The obtained results showed that the influence of the surface layer greatly modifies the potential distribution on the cross section and raises the voltage output of bent GaN NWs by up to 120%. In particular, the contribution from the surface piezoelectricity to the surface effect is found to be predominant over that of the surface elasticity and surface stresses.**

***Index Terms*—Electrostatic potential, finite element analysis, gallium nitride (GaN) nanowire (NW), molecular dynamics, surface effect.**

I. Introduction

SEMICONDUCTING nanomaterials are promising for the building blocks of nanoelectronics and nanodevices. Among them, zinc oxide (ZnO) and gallium nitride (GaN) demonstrate piezoelectric effects due to their wurtzite molecular structures. The unique synergy of semiconducting and piezoelectric properties makes them good candidates for constructing the newly promoted nanopiezoelectronics [1]–[3]. In particular, piezoelectric nanowire (NW)-based nanogenerators are considered as a breakthrough in developing nanoenergy harvesting devices and wireless (self-powered) nanomachines. In such nanogenerators, the voltage output originates from the transverse potential difference created on the cross section of the NWs due to the bending deformation along axial direction. It is thus of great interest to develop a mechanics model that accounts for the work mechanisms of the nanogenerators and enables one to achieve an accurate measurement of the voltage output and the potential distribution on their cross sections.

In earlier studies, the classical continuum mechanics and electromechanics theories were directly used as cost-effective methods for measuring these quantities analytically and/or numerically [1], [4]–[7]. When using the piezoelectric properties measured for GaN NW, Minary-Jolandan *et al.* [8] found that the maximum voltage obtained for bent GaN NWs were several times of those calculated based on the bulk piezoelectric properties. The stronger electromechanical response at the nanoscale was attributed to the enhanced effect of the surface layers of the NWs, which finally leads to the size-dependent material properties and thus challenges the classical continuum theories. For elastic nanomaterials, such a surface effect was explained in terms of the surface residual stress and surface elasticity [9]–[12], while for piezoelectric nanomaterials the surface piezoelectricity was also considered [13]–[19]. To qualitatively evaluate the surface effect the core-surface model (surface thickness $h = 0$) [9]–[19] and the core-shell (CS) model (surface thickness $h \neq 0$) [20]–[22] have been proposed for the nanostructures of different configurations, e.g., NWs [14], [15] and nanofilms [16], [17].

In this paper, we aim to examine the surface effect on the voltage output of GaN NW-based nanogenerators by considering the surface elasticity and surface piezoelectricity of the NWs. To this end, a 3-D composite beam model was developed where the piezoelectric NWs are considered as a 3-D composite beam comprising an inner solid beam and an outer hollow beam. The elastic and piezoelectric properties were then measured for the two components based on the molecular dynamics simulations (MDS) and the existing CS model. Finally, the finite element method (FEM) was utilized to calculate the bending deflection, the potential distribution and the voltage output of a bent GaN NW based on the obtained model and material properties.

II. Methodology

In this section, we will introduce the analysis methods for electrostatic potential generated in a bent GaN NW. First, the equivalent material properties of the surface layer and the core section of the NWs were measured by fitting an existing CS model to the MDS performed here. The obtained data were then inserted into a 3-D composite beam model developed in this study, which enables one to calculate the electrostatic potential generated in a bent GaN NW. The calculation was implemented by using the FEM. Here, it is noted that the cross sections of synthesized GaN NWs could be of different shapes, such as, square (or rectangle), triangle, hexagon, and circle [23], [24]. The shape variation, however, cannot affect the physics of the

Manuscript received June 18, 2013; revised February 21, 2014; accepted March 24, 2014. Date of publication March 27, 2014; date of current version May 6, 2014. The review of this paper was arranged by Associate Editor E. Tutuc.

The authors are with the College of Engineering, Swansea University, Swansea, Wales SA2 8PP, U.K. (e-mail: zjdyd1986@163.com; Chengyuan.Wang@swansea.ac.uk; s.adhikari@swansea.ac.uk).

Color versions of one or more of the figures in this paper are available online at http://ieeexplore.ieee.org.

Digital Object Identifier 10.1109/TNANO.2014.2313837

electromechanical responses studied and will not qualitatively change the surface effect on the potential output generated on the NWs. Thus, to simplify our analysis without losing generosity, in this study we considered square GaN NWs with the growth direction along c-axis [0001].

A. Evaluation of the Surface Material Properties and Thickness

In this study, MDS was employed to calculate the equivalent elastic and piezoelectric properties of GaN NWs. In the MDS, the interactions between Ga-Ga, N-N, and Ga-N were described by the Stillinger–Weber (SW) potential [25], which was employed to evaluate the elastic properties of hexagonal GaN NWs in [26] and [27]. The NVT ensemble (constant number of particles, volume, and temperature) was employed to update the positions and velocities of the atoms after each time step by using the Nosé–Hoover temperature thermostat [28]. At the beginning of all simulations, the equilibrium of the initialized structure was achieved corresponding to the lowest energy of the NWs. Here all MDS were conducted using the large-scale atomic/molecular massively parallel simulator [29] without the periodic boundary conditions.

To measure the equivalent Young's modulus of the NWs the MDS was performed at room temperature ($T = 300$ K), where one end of the NWs was fixed while the other end was pulled along the axial direction with the maximum strain $\varepsilon = 0.01$. In this process, the σ (tensile stress)—ε (axial strain) curve was recorded, where the slope gives the equivalent Young's modulus E. In the study of the piezoelectric effect on GaN NWs, one noted that for the c-axis NWs, the voltage on their cross sections due to bending is primarily a result of the piezoelectric effect in the axial direction [1], [8], [30], which is characterized by the piezoelectric constant e_{33}. Thus, in this study, we measured e_{33} based on MDS. For the details of the MDS readers may refer to our recent paper [19].

The CS model was used to account for the size-dependent material properties of NWs in terms of their surface material properties and the surface thickness. In the CS model, a square cross-sectional NW with the cross-section size b is treated as a composite beam comprising a surface layer with thickness h, Young's modulus E_s and piezoelectric property e_{33}^s, and an inner section of Young's modulus E_b and piezoelectric property e_{33}^b. The elementary mechanics theory of composite materials gives (see Appendix A)

$$E = E_b + 4\frac{(E_s - E_b)\,h}{b}\left(1 - \frac{h}{b}\right) \tag{1}$$

$$e_{33} = e_{33}^b + 4\frac{\left(e_{33}^s - e_{33}^b\right)h}{b}\left(1 - \frac{h}{b}\right). \tag{2}$$

Fitting (1) and (2), respectively, to the equivalent E and e_{33} obtained in the MDS yields the values of $E_b, E_s, e_{33}^b, e_{33}^s$ and the effective thickness h. Here it should be pointed out that, in (1) and (2) the four lateral surfaces of square GaN NWs are considered. Among them, the perpendicular surfaces are in the different crystal planes and thus may have different material properties. However, in (1) and (2), the material properties are assumed to be isotropic for the surfaces of the GaN NWs. As will be shown later, such a simplified model can still give a reliable description to the overall mechanical and piezoelectric responses of NWs.

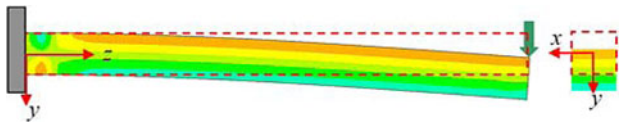

Fig. 1. Sketch of a piezoelectric nanogenerator. The NW is pushed toward the positive direction of the y-axis by a lateral force acting on its free end. The bending results in a potential distribution in the NW almost independent of the z-coordinate (c-axis).

B. Three-Dimensional Composite Beam Model for Piezoelectric NWs

The configuration of a piezoelectric nanogenerator is illustrated in Fig. 1, where a GaN piezoelectric NW is attached to a substrate at one end and scanned over at the other (free) end by the tip of an atomic force microscope (AFM). The lateral force applied on the free end gives rise to the mechanical deflection and piezoelectric polarization of the NW. Based on the theory of piezoelectricity, negative potential is generated on the compressed side of the bent NW while positive one is induced on the stretched side (see Fig. 1). Thus, the electrical potential varies substantially across the cross section of the bent NW. In this paper, our objective was to calculate the potential distribution on the cross section of bent GaN NWs. To account for the effect of the surface layer we considered the NWs as 3-D composite beams comprising an inner solid beam and an outer hollow beam. The theoretical framework for such a 3-D composite beam model is detailed as follows.

First, the inner solid beam is made of bulk material and its constitutive equations read

$$\sigma_{ij}^b = c_{ijkl}^b \varepsilon_{kl}^b - e_{ijk}^b E_k \;(i,j,k,l = 1,2,3) \tag{3}$$

$$D_i^b = e_{kli}^b \varepsilon_{kl}^b + k_{ik}^b E_k \tag{4}$$

where σ_{ij}^b and ε_{kl}^b are the bulk stress and strain tensor, respectively. D_i^b and E_k are the bulk electric displacement and the electric field. c_{ijkl}^b, e_{ijk}^b, and k_{ik}^b are the bulk elastic coefficient, piezoelectric coefficient, and dielectric constant, respectively. The extended matrix forms of $c_{ijkl}^b, e_{ijk}^b, k_{ik}^b$ are shown in Appendix B. Also as shown in Appendix B, the nonzero elements of c_{ijkl}^b are the functions of Young's modulus E_b (1) and Poisson ratio v, and the only elements of e_{ijk}^b required in this study is e_{33}^b. Here stress σ_{ij}^b, strain ε_{kl}^b and electric displacement D_i^b of the inner section have to satisfy the equilibrium equations (5), the compatibility equation (6), and the Gauss equation (7) shown as follows [4]:

$$\sigma_{ij,j}^b = 0 \tag{5}$$

$$\varepsilon_{il,jk}^b + \varepsilon_{jk,il}^b - \varepsilon_{ik,jl}^b - \varepsilon_{jl,ik}^b = 0 \tag{6}$$

$$D_{i,i}^b = 0 \tag{7}$$

where a comma represents differentiation with respect to the coordinate.

Second, for the outer hollow beam made of the surface material, the constitutive equations become [13]

$$\sigma_{ij}^{s} = \sigma_{ij}^{0} + c_{ijkl}^{s}\varepsilon_{kl}^{s} - e_{ijk}^{s}E_{k} \tag{8}$$

$$D_{i}^{s} = D_{i}^{0} + e_{kli}^{s}\varepsilon_{kl}^{s} + k_{ik}^{s}E_{k}. \tag{9}$$

Here the notations of (3) and (4) are used for the same quantity but subscript b in (3) and (4) are replaced by s to represent the surface layers (or shell component). In addition, σ_{ij}^{0} is the residual surface stress and initial D_{i}^{0} is the surface electric displacement due to σ_{ij}^{0}. Again $\sigma_{ij}^{s}, \varepsilon_{kl}^{s}$, and D_{i}^{s} in (8) and (9) must satisfy the corresponding equilibrium equations, compatibility equations, and Gauss equation, respectively. For the surface layers, those equations as well as the extended forms of material constants can be obtained from their counterparts of the core section by replacing the superscript b with s. Thus, similar to the inner section, the nonzero elements of c_{ijkl}^{s} can be calculated based on Young's modulus E_s (1) and Poisson ratio (assumed to be the same as that of the core section), and the only element of e_{ijk}^{s} required for the calculation is e_{33}^{s}. Here, it should be noted that while (E_s, e_{33}^{s}) and (E_b, e_{33}^{b}) are different for the two components of the NWs and determined in Section II-A by fitting (1) and (2) to the MDS, the Poisson ratio of the two parts are assumed to be the same as the bulk value that can be obtained in the literature. In addition, an experiment [31] showed that the dielectric constant of piezoelectric NWs was also size-dependent but the surface dielectric constant of GaN NWs is still absent in the literature. Thus, following previous studies [32] we assumed $k_{ik}^{s} = k_{ik}^{b}$ (bulk value) in this paper.

Further, σ_{ij}^{0} in (8) was neglected for the following reasons. 1) The charges or the surface electric displacement D_{i}^{0} generated by σ_{ij}^{0} will be released once the AFM tip touches the NW and cannot be reproduced. 2) The equilibrium of an NW requires that, initially the core section is subjected to a compressive stress to balance the surface tension σ_{ij}^{0}. It is shown that such a distributed residual stress on the cross section has no influence on the transverse deflection of the NW [12], [33] and accordingly, their strains due to the deflection [1].

Moreover, in the 3-D composite beam model, the continuity conditions are applied to the interface between the inner solid beam and outer hollow beam, which requires that the strain and the electric field of the two components are exactly the same on their interface. Based on (4)–(7) of the inner beam, their counterparts of the outer beam and the continuity condition on the interface one is able to solve the problems to obtain the electric potential on the cross section of the bent GaN NWs. In this study, all calculations were carried out based on the FEM and implemented via ANSYS, a widely used FEM software.

III. Results and Discussion

Following the methods demonstrated in Section II, we have calculated the material properties and thickness of the surface layer and subsequently computed the potential distribution in the bent GaN NWs.

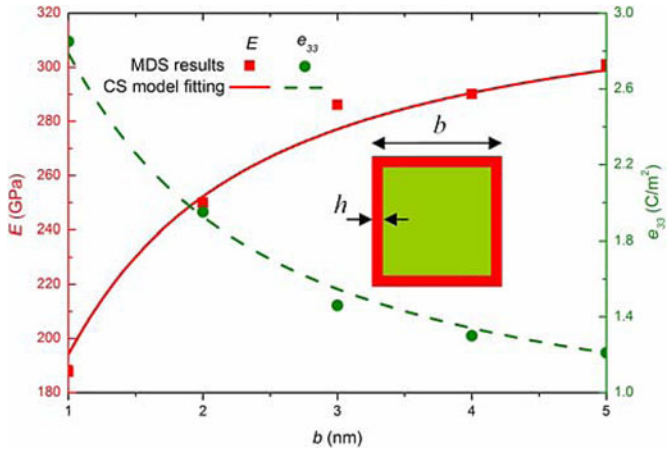

Fig. 2. Equivalent Young's modulus and the piezoelectric constant e_{33} of GaN NWs as a function of the cross section size b. The results are obtained based on MDS and the CS model. The inset shows the CS model where h is the thickness of the surface layer.

TABLE I
Elastic and Piezoelectric Properties, and the Surface Thickness of the GaN NWs Predicted Based on the CS Model and the Present MDS (Young's Modulus ($\bar{E}$) and Piezoelectric Property ($\bar{e}_{33}$) of the Bulk GaN [36, 37] Are Also Listed Here)

Property	Value
E_b (GPa)	335
$\bar{E}$ (GPa)	311 [36]
E_s (GPa)	152
e_{33}^{b} (C/m^2)	0.65
$\bar{e}_{33}$ (C/m^2)	0.67 [37]
e_{33}^{s} (C/m^2)	3.3
h (nm)	0.26[a]/0.28[b]

The Young's modulus ($\bar{E}$) and piezoelectric property ($\bar{e}_{33}$) of the bulk GaN [36, 37] are also listed here.

[a] the thickness of the elastic surface layer;

[b] the thickness of the piezoelectric surface layer.

A. Material Properties and Thickness of the Surface Layer

First, we measured the equivalent Young's modulus E and piezoelectric constant e_{33} of the NWs based on MDS and then extracted the equivalent material properties and effective thickness of the surface layer by fitting the CS model to MDS. The equivalent Young's modulus and piezoelectric constants e_{33} are shown in Fig. 2 for a group of GaN NWs whose length L is fixed at 15 nm and the size b of the square cross section varies from 1 to 5 nm. It is seen from Fig. 2 that the equivalent Young's modulus E decreases as the cross-sectional size b decreases. This tendency is found to be consistent with those obtained in previous experiment [34] and atomistic simulations [27] for GaN NWs. The dependence of e_{33} on b was also plotted in Fig. 2 where e_{33} increases with the decreasing b. Similar observation was reported in the first-principle calculations [35] and the experiment [8]. The results obtained from the curve fitting in Fig. 2 are summarized in Table I in comparison with the existing bulk

values [36], [37]. The table shows that the equivalent elastic and piezoelectric properties obtained for the inner section of the NWs are very close to the corresponding bulk values reported in existing simulations, whereas those of surface layers are substantially different. These results indicate that the structural changes on the surface layer are significant and lead to the elastic and piezoelectric properties differing from the bulk values.

B. Surface Effects on the Deflection, Voltage Output, and Potential Distribution

In this section, the potential output for a bent ZnO NW considered previously in [4] and [6] was first tested to validate our present method and model. In the calculation the material properties and the geometric size are the same as those in [4] and [6]. Specifically, for the sake of comparison, the effect of the surface layer was completed excluded in this particular case and the calculations were done based on the classical mechanics and electromechanics theories, i.e., (3) to (7), used in [4] and [6]. The voltage output V given by our FEM analysis is 0.3 V, which is found to be in perfect agreement with 0.3 V reported in [6] and very close to 0.28 V obtained in [4].

Subsequently, we carried out the analyses based on the present 3-D composite beam model (accounting for the surface effects) for GaN NWs bent by a lateral force The length of the NWs is fixed at $L = 120$ nm but the size b of their square cross-sections ranges from 8 to 20 nm. In all examples, the lateral force was set as 20 nN. Here our goal is to examine the surface effects on the mechanical and electrical responses of the bent GaN NWs. Thus, for the sake of comparison the classical theory based on (3) to (7) only was also used to get the results for the NWs without the surface effect. Most of the material properties and the effective thickness of the surface layer required for the calculation were obtained in Table I. In addition, $\nu = 0.183$ [38], $k^s_{11} = k^b_{11} = 10.4$, and $k^s_{33} = k^b_{33} = 9.7$ [39] were used for both parts of the NWs.

Under the same lateral force Fig. 3(a) shows the deflection f of the NWs as a function of the cross-sectional size b. It is observed that f decreases with increasing b as the structural stiffness of the NWs becomes greater in this process. In particular, the deflection f obtained by considering surface effects is larger than the one calculated without considering surface effects. This observation can be attributed to the softening effect of the surface layer on the elastic modulus of NWs, i.e., the effect of the surface elasticity (see Fig. 2). To further examine the influence of the surface effects on f we have plotted the deflection ratio α in Fig. 3(a), which is defined as the deflection with surface effects normalized by the deflection without surface effects. It is seen that the surface effects on f decrease as the cross-sectional size increases. For example, at $b = 8$ nm α is 1.14, i.e., f is raised by 14% due to the surface effect but it decreases to around 1.07 at $b = 20$ nm, i.e., f is raised only by 7% due to the surface effect. From these results it follows that the surface effects on the deflection of the bent GaN NWs is significant but it fades away rapidly with rising b.

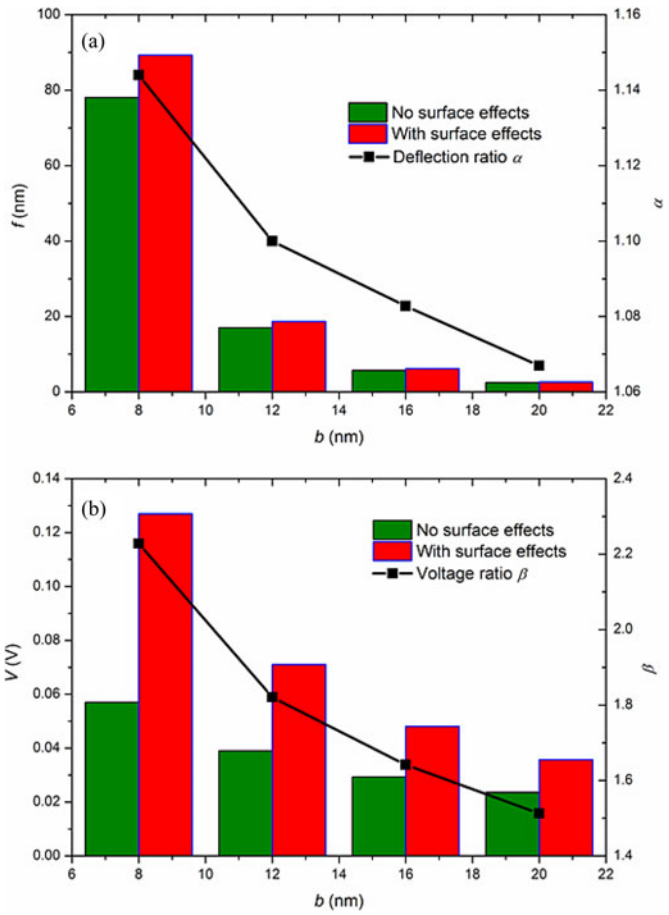

Fig. 3. (a) Transverse deflection f and the deflection ratio α of the GaN NW as a function of the cross-section size b. (b) Voltage output V and the voltage ratio β of the NW as a function of b.

In Fig. 3(b), the voltage output V was computed for the GaN NWs against the cross-sectional size b. It is seen from the figure that V decreases as b grows and V with surface effects is larger than the one without surface effects. To qualitatively measure the surface effect on V we have defined the voltage (with surface effects)-to-voltage (without surface effects) ratio β. Such a voltage ratio was then calculated in Fig. 3(b) where cross-sectional size b decreases from 20 to 8 nm. In this process, it is found that β is raised from 1.5 to more than 2.2, which correspond to V increases from 50% to more than 120%. Based on these results we come to the conclusions that the surface effect is substantial on the voltage output and thus has to be taken into consideration in the design of nanogenerators. In other words, the classical theory greatly underestimates the voltage output of bent NWs and accordingly, the performance of the nanogenerators. Moreover, comparing the 50% to 120% voltage increase with the 7% to 14% deflection increase (due to the surface elasticity only), one can come to the conclusion (also will be shown in Section III-C) that the surface piezoelectricity plays a predominant role over the surface elasticity in determining the voltage output of the NWs. Such a size-hardening effect on V was also observed in an experimental study [8], but the size-hardening effect obtained is much greater than the effect

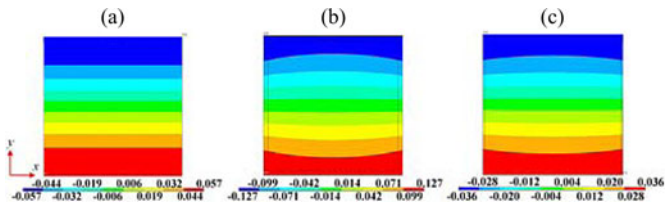

Fig. 4. Cross-sectional potential distribution of bent GaN NWs. (a) $b = 8$ nm without surface effects. (b) $b = 8$ nm with surface effects. (c) $b = 20$ nm with surface effects.

given by the present mechanics model. For example β observed in [8] was up to 3 for NWs with thickness in 65 to 160 nm, while in this study, β is expected to be smaller than 1.5 for NWs of the same size. Indeed, further studies are required to examine this issue and provide a theoretical explanation for the quantitative disagreement.

In addition, the surface effects on the cross-sectional potential distribution in a bent GaN NW was further studied in Fig. 4. The results are shown in Fig. 4(a) for the NW without considering surface effects, and Fig. 4(b) and (c) for the NW with surface effects and $b = 8$ nm and 20 nm, respectively. It is observed in Fig. 4(a) that when the surface effects are neglected the potential distributes uniformly along the x-axis, i.e., the electrical potential on the cross section varies with the y-coordinate along which bending occurs but is independent of x-coordinate (see Figs. 1 and 4). On the other hand, when the surface effects are considered [see Fig. 4(b) and (c)] the potential changes not only in the y-axis direction but also varies gradually along the x-axis at the top and bottom of the cross section. Comparison between Fig. 4(c) and (b) shows that as the cross-sectional size b of the NW increases from 8 to 20 nm the influence of the surface layer becomes less pronounced on the potential distribution along the x-axis.

C. Physical Mechanisms of the Surface Effect

In principle, the surface effect is the resultant effect of the surface elasticity and surface piezoelectricity. To achieve better understanding of the surface effects observed in Section III-B, we shall estimate the contributions of these two individual factors to the resultant surface effects. To this end the voltage ratio β was calculated with 1) $c^s_{ijkl} = c^b_{ijkl}, e^s_{ijk} \neq e^b_{ijk}$ to measure the effect of surface piezoelectricity, 2) $c^s_{ijkl} \neq c^b_{ijkl}, e^s_{ijk} = e^b_{ijk}$ to measure the effect of surface elasticity, and 3) $c^s_{ijkl} \neq c^b_{ijkl}, e^s_{ijk} \neq e^b_{ijk}$ to quantify the resultant effect of both factors. The results are plotted in Fig. 5 for the NWs of different cross-sectional size b. It is seen from Fig. 5 that both surface elasticity and surface piezoelectricity enhance the voltage output V and the effects turn out to be more significant for the NWs with smaller cross-sectional size b. Furthermore, it is also noted in the figure that the influence of the surface piezoelectricity is much stronger than that of the surface elasticity. For example, at $b = 20$ nm the surface elasticity only raise V by 6%, while the surface piezoelectricity increases it by 43% that is seven times as much as the increase due to the surface elasticity. Similar result can also be observed in Fig. 5 for the NWs of $b = 8$ nm.

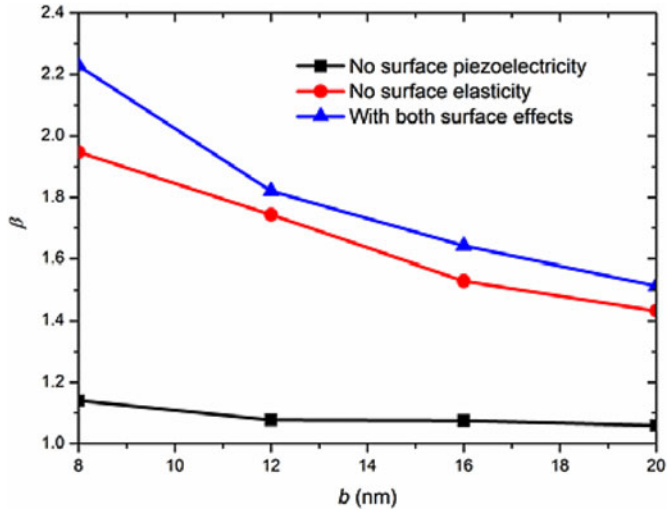

Fig. 5. Voltage ratio β calculated for the NWs of different cross-section size b. Here rectangles represent the results obtained without considering surface piezoelectricity, circles denote the results where only the surface piezoelectricity is considered and triangles give the data where both the surface piezoelectricity and surface elasticity are considered.

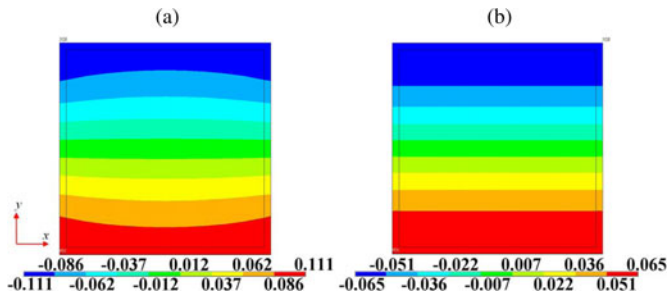

Fig. 6. Cross-sectional potential distribution calculated for a bent GaN NW of $b = 8$ nm by considering (a) the surface piezoelectricity and (b) the surface elasticity, respectively.

Next let us examine the effect of surface elasticity and surface piezoelectricity on the potential distribution in the bent GaN NW individually. In doing this, we calculated the potential distribution in the bent GaN NWs by considering case 1) $c^s_{ijkl} = c^b_{ijkl}, e^s_{ijk} \neq e^b_{ijk}$ and 2) $c^s_{ijkl} \neq c^b_{ijkl}, e^s_{ijk} = e^b_{ijk}$ in Fig. 6(a) and (b), respectively. Here $b = 8$ nm was considered for the NWs. We can see from Fig. 6 that, in case (1) where only the surface elasticity is considered, the potential distribute uniformly along the x-axis, which is the nearly same as that of the NW without surface effects [see Fig. 4(a)]. On the contrary, in case (2) where only surface piezoelectricity is involved the potential distribution is found to vary significantly along the x-axis. The potential distribution is very similar to that of the NW where both surface elasticity and piezoelectricity were taken into consideration [see Fig. 4(b)]. These results show clear evidence that the potential distribution is affected predominantly by the surface piezoelectricity. Form these results it follows that the surface layer would raise the voltage output and change the potential distribution of the GaN NW-based nanogenerators primarily via the influence of the surface piezoelectricity.

IV. Conclusion

The surface effects have been examined for mechanical and piezoelectric responses of bent GaN NWs, including the transverse deflection, voltage output, and the potential distribution. The study was carried out based on a 3-D composite beam comprising an inner solid beam and an outer hollow beam implemented by using FEM. It is essential to determine the equivalent material properties of the different sections and the thickness of the outer section for NWs modeled as 3-D composite beam. To this end MDS were first carried out to measure the overall material properties for NW samples with different thickness. The 3-D composite beam model will then be fitted to these MDS-derived parameters to extract the values of required material properties and the outer layer thickness. The major conclusions drawn in this study are summarized as follows.

1) The equivalent Young's modulus of the GaN NWs decreases with decreasing cross-sectional size and is lower than its bulk counterpart. Differently, the piezoelectric constant rises with decreasing cross-sectional size and is greater than the bulk value.
2) When the same lateral force is concerned, the surface effects enhance the voltage output and the transverse deflection of the bent GaN NWs. The potential distribution of the NWs can also be altered significantly due to the surface effect. In particular, for the NWs considered here the surface effects raise the voltage output by 50% to 120% which is six to eight times of 7% to 14% increase in the transverse deflection.
3) The surface effects on the voltage output and the potential distribution mainly originate from the effect of the surface piezoelectricity. The effect of the surface elasticity is significant but much smaller than that of the surface piezoelectricity.

These conclusions suggest that the surface effect ignored in the previous calculations has to be considered in the design of the nanogenerators. Specifically, it is clearly seen that as a result of the surface effect the finer piezoelectric NWs can generate much greater voltage output than the coarse ones. These results are expected to provide an important guideline for the design and applications of the nanogenerators. On the other hand, the effect of the surface dielectricity was completely neglected in this analysis due to lack of experimental and simulation data. Such an effect, however, could be significant and thus deserves further study in the near future.

Appendix

I. Effective Elastic and Piezoelectric Constants of NWs

For an NW under tension ε we can obtain

$$EA\varepsilon = E_b A_{in}\varepsilon + E_s A_s \varepsilon \tag{A1}$$

where A, A_{in}, and A_s, respectively, are the cross-section area of the whole NW, the inner section and the surface; and E, E_b, and E_s are, respectively, Young's modulus of the whole NW, the inner section and the surface.

For a square cross section with thickness b and surface thickness h it is written as

$$Eb^2 = E_b(b-2h)^2 + E_s[b^2 - (b-2h)^2] \tag{A2}$$

which leads to the effective Young's modulus under tension as

$$E = E_b + 4(E_s - E_b)\left[\frac{h}{b} - \left(\frac{h}{b}\right)^2\right]. \tag{A3}$$

When an NW under an axial electric field E_3 from the composite beam theory we yield

$$e_{33}AE_3 = e^b_{33}A_{in}E_3 + e^s_{33}A_sE_3 \tag{A4}$$

where e_{33}, e^b_{33}, and e^s_{33} are, respectively, the piezoelectric constants of the whole NW, the inner section and the surface.

For an NW with a square cross section the effective piezoelectric constant is

$$e_{33} = e^b_{33} + 4(e^s_{33} - e^b_{33})\left[\frac{h}{b} - \left(\frac{h}{b}\right)^2\right]. \tag{A5}$$

II. Extended Matrix Forms of $c^b_{ijkl}, e^b_{ijk}, k^b_{ik}$

It should be noted that the subscripts in the material constants as shown in (3) and (4) can be relabeled in the contracted notation due to the symmetry of stress and strain tensors following $11 \to 1$; $22 \to 2$; $33 \to 3$; $23 \to 4$; $13 \to 5$; $12 \to 6$. Thus elastic coefficient, especially for isotropic materials can be expressed as

$$c^b_{pq} = \begin{pmatrix} c^b_{11} & c^b_{12} & c^b_{13} & 0 & 0 & 0 \\ c^b_{21} & c^b_{22} & c^b_{23} & 0 & 0 & 0 \\ c^b_{31} & c^b_{32} & c^b_{33} & 0 & 0 & 0 \\ 0 & 0 & 0 & c^b_{44} & 0 & 0 \\ 0 & 0 & 0 & 0 & c^b_{55} & 0 \\ 0 & 0 & 0 & 0 & 0 & c^b_{66} \end{pmatrix} = \frac{E_b}{2(1-\nu^2)} \begin{pmatrix} 2 & 2\nu & 2\nu & 0 & 0 & 0 \\ 2\nu & 2 & 2\nu & 0 & 0 & 0 \\ 2\nu & 2\nu & 2 & 0 & 0 & 0 \\ 0 & 0 & 0 & 1-\nu & 0 & 0 \\ 0 & 0 & 0 & 0 & 1-\nu & 0 \\ 0 & 0 & 0 & 0 & 0 & 1-\nu \end{pmatrix} \tag{A6}$$

where $p, q = 1, 2, \ldots, 6$.

The piezoelectric coefficient and the dielectric constant can be expressed as

$$e^b_{kp} = \begin{pmatrix} 0 & 0 & 0 & 0 & e^b_{15} & 0 \\ 0 & 0 & 0 & e^b_{15} & 0 & 0 \\ e^b_{31} & e^b_{32} & e^b_{33} & 0 & 0 & 0 \end{pmatrix} \tag{A7}$$

$$k^b_{ik} = \begin{pmatrix} k^b_{11} & 0 & 0 \\ 0 & k^b_{11} & 0 \\ 0 & 0 & k^b_{33} \end{pmatrix}. \tag{A8}$$

ACKNOWLEDGMENT

J. Zhang acknowledges the support from the China Scholarship Council. S. Adhikari acknowledges the support from the Royal Society through the award of Wolfson Research Merit Award.

REFERENCES

[1] Z. L. Wang and J. H. Song, "Piezoelectric nanogenerators based on zinc oxide nanowire arrays," *Science*, vol. 312, pp. 242–246, 2006.

[2] P. X. Gao, J. H. Song, J. Liu, and Z. L. Wang, "Nanowire piezoelectric nanogenerators on plastic substrates as flexible power sources for nanodevices," *Adv. Mater.*, vol. 19, pp. 67–72, 2007.

[3] J. H. Song, J. Zhou, and Z. L. Wang, "Piezoelectric and semiconducting coupled power generating process of a single ZnO belt/wire: A technology for harvesting electricity from the environment," *Nano Lett.*, vol. 6, pp. 1656–1662, 2006.

[4] Y. Gao and Z. L. Wang, "Electrostatic potential in a bent piezoelectric nanowire: The fundamental theory of nanogenerator and nanopiezotronics," *Nano Lett.*, vol. 7, pp. 2499–2505, 2007.

[5] C. Falconi, G. Mantinia, A. D. Amico, and Z. L. Wang, "Studying piezoelectric nanowires and nanowalls for energy harvesting," *Sens. Actuators B*, vol. 139, pp. 511-519, 2009.

[6] M. A. Schubert, S. Senz, M. Alexe, D. Hesse, and U. Gosele, "Finite element method calculations of ZnO nanowires for nanogenerators," *Appl. Phys. Lett.*, vol. 92, pp. 122904-1–122904-3, 2008.

[7] Z. Z. Shao, L. Y. Wen, D. M. Wu, X. A. Zhang, S. L. Chang, and S. Q. Qin, "Influence of carrier concentration on piezoelectric potential in a bent ZnO nanorod," *J. Appl. Phys.*, vol. 108, pp. 124312-1–124312-5, 2010.

[8] M. Minary-Jolandan, R. A. Bernal, I. Kuljanishvili, V. Parpoil, and H. D. Espinosa, "Individual GaN nanowires exhibit strong piezoelectricity," *3D Nano Lett.*, vol. 12, pp. 970–976, 2012.

[9] R. E. Miller and V. B. Shenoy, "Size-dependent elastic properties of nanosized structural elements," *Nanotechnology*, vol. 11, pp. 139–147, 2000.

[10] M. E. Gurtin and A. I. Murdoch, "A continuum theory of elastic material surfaces," *Arch. Ration. Mech. Anal.*, vol. 57, pp. 291–323, 1975.

[11] G. F. Wang and X. Q. Feng, "Effects of surface elasticity and residual surface tension on the natural frequency of microbeams," *Appl. Phys. Lett.*, vol. 90, pp. 231904-1–231904-3, 2007.

[12] J. Zhang, C. Y. Wang, R. Chowdhury, and S. Adhikari, "Small-scale effect on the mechanical properties of metallic nanotubes," *Appl. Phys. Lett.*, vol. 101, pp. 093109-1–093109-4, 2012.

[13] G. Y. Huang and S. W. Yu, "Effect of surface piezoelectricity on the electromechanical behaviour of a piezoelectric ring," *Phys. Status Solidi B.*, vol. 243, pp. R22–R24, 2006.

[14] Z. Yan and L. Y. Jiang, "Surface effects on the electromechanical coupling and bending behaviours of piezoelectric nanowires," *J. Phys. D: Appl. Phys.*, vol. 44, pp. 075404-1–075404-6, 2010.

[15] Z. Yan and L. Y. Jiang, "The vibrational and buckling behaviors of piezoelectric nanobeams with surface effects," *Nanotechnology*, vol. 22, pp. 245703-1–245703-7, 2011.

[16] J. Zhang and C. Y. Wang, "Vibrating piezoelectric nanofilms as sandwich nanoplates," *J. Appl. Phys.*, vol. 111, pp. 094303-1–094303-6, 2012.

[17] J. Zhang, C. Y. Wang, and S. Adhikari, "Surface effect on the buckling of piezoelectric nanofilms," *J. Phys. D: Appl. Phys.*, vol. 45, pp. 285301-1–285301-8, 2012.

[18] S. X. Dai, M. Gharbi, P. Sharma, and H. S. Park, "Surface piezoelectricity: Size effects in nanostructures and the emergence of piezoelectricity in non-piezoelectric materials," *J. Appl. Phys.*, vol. 110, pp. 104305-1–104305-7, 2011.

[19] J. Zhang, C. Y. Wang, R. Chowdhury, and S. Adhikari, "Size and temperature dependent piezoelectric properties of gallium nitride nanowires," *Scripta Mater.*, vol. 68, pp. 627–630, 2013.

[20] C. Q. Chen, Y. Shi, J. Zhu, and Y. J. Yan, "Size dependence of Young's modulus in ZnO nanowires," *Phys. Rev. Lett.*,, vol. 96, pp. 075505-1–075505-4, 2006.

[21] G. Stan, C. V. Ciobanu, P. M. Parthangal, and R. F. Cook, "Diameter-dependent radial and tangential elastic moduli of ZnO nanowires," *Nano Lett.*, vol. 7, pp. 3691–3697, 2007.

[22] M. R. He, Y. Shi, W. Zhou, J. W. Chen, Y. J. Yan, and J. Zhu, "Diameter dependence of modulus in zinc oxide nanowires and the effect of loading mode: In situ experiments and universal core-shell approach," *Appl. Phys. Lett.*, vol. 95, pp. 091912-1–091912-3, 2009.

[23] S. Barth, F. Hernandez-Ramirez, J. D. Holmes, and A. Romano-Rodriguez, "Synthesis and applications of one-dimensional semiconductors," *Prog. Mater. Sci.*, vol. 55, pp. 563–627, 2010.

[24] R. Yu, L. Dong, C. Pan, S. Niu, H. Liu, W. Liu, S. Chua, D. Chi, and Z. L. Wang, "Piezotronic effect on the transport properties of GaN nanobelts for active flexible electronics," *Adv. Mater.*, vol. 24, pp. 3532–3537, 2012.

[25] F. H. Stillinger and T. A. Weber, "Computer simulation of local order in condensed phases of silicon," *Phys. Rev. B*, vol. 31, pp. 5262–5271, 1985.

[26] R. A. Bernal, R. Agrawal, B. Peng, K. A. Bertness, N. A. Sanford, A. V. Davydov, and H. D. Espinosa, "Effect of growth orientation and diameter on the elasticity of GaN nanowires: A combined in situ TEM and atomistic modeling investigation," *Nano Lett.*, vol. 11, pp. 548–555, 2011.

[27] Z. G. Wang, X. T. Zu, L. Yang, F. Gao, and W. J. Weber, "Atomistic simulations of the size, orientation, and temperature dependence of tensile behavior in GaN nanowires," *Phys. Rev. B*, vol. 76, pp. 045310-1–045310-9, 2007.

[28] S. Nosé, "A unified formulation of the constant temperature molecular dynamics methods," *J. Chem. Phys.*, vol. 81, pp. 511–519, 1984.

[29] S. J. Plimpton, "Fast parallel algorithms for short-range molecular dynamics," *J. Comput. Phys.*, vol. 117, pp. 1–19, 1995.

[30] X. Wang, J. Song, F. Zhang, C. He, Z. Hu, and Z. L. Wang, "Electricity generation based on one-dimensional group-III nitride nanomaterials," *Adv. Mater.*, vol. 22, pp. 2155–2158, 2010.

[31] Y. Yang, W. Guo, X. Wang, Z. Wang, J. Qie, and Y. Zhang, "Size dependence of dielectric constant in a single pencil-like ZnO nanowire," *Nano Lett.*, vol. 12, pp. 1919–1922, 2012.

[32] H. Yao, G. Yun, and N. Bai, "Influence of exponentially increasing surface elasticity on the piezoelectric potential of a bent ZnO nanowire," *J. Phys. D: Appl. Phys.*, vol. 45, pp. 285304-1–285304-7, 2012.

[33] F. Song, G. L. Huang, H. S. Park, and X. N. Liu, "A continuum model for the mechanical behavior of nanowires including surface and surface-induced initial stresses," *Int. J. Solid Struct.*, vol. 48, pp. 2154–2163, 2011.

[34] C. Y. Nam, P. Jaroenapibal, D. Tham, D. E. Luzzi, S. Evoy, and J. E. Fischer, "Diameter-dependent electromechanical properties of GaN nanowires," *Nano Lett.*, vol. 6, pp. 153–158, 2006.

[35] R. Agrawal and H. D. Espinosa, "Giant piezoelectric size effects in zinc oxide and gallium nitride nanowires: A first principles investigation," *Nano Lett.*, vol. 11, pp. 786–790, 2011.

[36] R. B. Schwarz and K. Khachaturyan, "Elastic moduli of gallium nitride," *Appl. Phys. Lett.*, vol. 70, pp. 1122–1124, 1997.

[37] F. Bernardini, V. Fiorentini, and D. Vanderbilt, "Accurate calculation of polarization-related quantities in semiconductors," *Phys. Rev. B*, vol. 63, pp. 193201-1–193201-4, 2001.

[38] M. A. Moram, Z. H. Barber, and C. J. Humphreys, "Accurate experimental determination of the Poisson's ratio of GaN using high-resolution x-ray diffraction," *J. Appl. Phys.*, vol. 102, pp. 023505-1–023505-4, 2007.

[39] M. E. Levinshtein, S. L. Rumyantsev, and M. S. Shur, *Properties of Advanced Semiconductor Materials: GaN, AlN, InN, BN, SiC, SiGe*. New York, NY, USA: Wiley, 2001.

Authors' photographs and biographies not available at the time of publication.